Electronic Supplementary Material (ESI) for Analyst.
This journal is © The Royal Society of Chemistry 2014

Supplementary Information

Rapid method to estimate the concentration of citrate capped silver nanoparticles from UV-visible light spectra

David Paramelle,[†] Anton Sadovoy,[†,] Sergey Gorelik,[†] Paul Free,[†,]* Jonathan Hobley,[†] David G. Fernig[‡]*

[†]Institute of Materials Research and Engineering, A*STAR (Agency for Science, Technology and Research), 3 Research Link, Singapore 117602.

[‡]Department of Biochemistry, Institute of Integrative Biology, University of Liverpool, Liverpool L69 7ZB, UK.

*Address correspondence to sadovoya@imre.a-star.edu.sg; freepf@a-star.edu.sg.

Table of Contents

Table S1. Table for determining molar concentration of spherical citrate-capped silver nanoparticles in water using UV-visible spectra.

The data of ε can be used to calculate the particle molar concentration c in mol per litre from the absorption A at the particles measured λ_{max}, using the Beer- Lambert law:

$c = A/\varepsilon$

The table compares the simulated molar decadic extinction coefficient (ε) of spherical citrate-capped silver nanoparticles with diameter d. Simulated λ_{max} values for citrate-coated silver nanoparticles are shown. Real silver nanoparticles have a size distribution typically up to +/- 5 %, and thus can have a λ_{max} bias towards higher wavelengths due to larger nanoparticles contributing more towards absorbance / scattering. This is demonstrated in figure S13, comparing simulated and experimental data of 75 nm spherical citrate-capped silver nanoparticles. Diameter is determined by TEM as %volume count. *Data estimated by extrapolation of measured points with power function $y = a(1 - x^{-b})$ in the size region from 8nm to 20nm (a = 405, b=3/2).

d / nm	λ_{max} / nm	ε / M^{-1} cm^{-1} $\cdot 10^8$	d / nm	λ_{max} / nm	ε / M^{-1} cm^{-1} $\cdot 10^8$
8	392.0*	1.84	56	427.0	658
10	392.1*	5.56	58	429.2	699
12	395.2*	10.1	60	431.5	739
14	397.2*	15.8	62	433.8	779
16	398.5*	22.7	64	436.2	820
18	399.7*	31.3	66	438.7	860
20	400.8	41.8	68	441.3	900
22	401.6	54.8	70	443.8	941
24	402.5	70.8	72	446.7	981
26	403.5	90.5	74	449.5	1021
28	404.5	115	76	452.3	1062
30	405.6	145	78	455.3	1102
32	406.8	181	80	458.3	1142
34	408.1	215	82	461.4	1183
36	409.4	255	84	464.6	1223
38	410.8	295	86	467.9	1263
40	412.3	336	88	471.2	1304
42	413.9	376	90	474.6	1344
44	415.5	416	92	478.1	1384
46	417.3	457	94	481.6	1425
48	419.1	497	96	485.3	1465
50	420.9	537	98	489.0	1505
52	422.9	578	100	492.8	1546
54	424.9	618			

Table S2. Parameters of silver nanoparticles supplied by manufacturer or obtained experimentally.

AgNPs size (manufacturer's batch code)	Manuf. TEM size (nm)	Manuf. Hydro-dynamic diameter (nm)	Manuf. λmax	Mean diameter (nm)[a] *[and S.D.]*	Mean diameter (nm)[b]	Average circularity[c]	Measured λmax
10 nm (JME1109)	8.40	N/A	391	8.40[d]			395
10 nm (DAG1094)	9.6	N/A	391	8.92 [1.84]	8.06	0.62	393
20 nm (JME1074)	20.8	32.0	401	19.02 [1.78]	18.60	0.73	404
20 nm (DAC1290)	22.44	25.5	403	19.75 [2.65]	18.92	0.70	404
30 nm (KJW1215)	32.3	44.8	406	30.40 [3.79]	29.26	0.91	405
40 nm (JME1114)	39.5	55.3	413	37.90 [3.10]	36.95	0.83	411
50 nm (JME1032)	49.1	59.2	418	45.93 [3.65]	45.11	0.84	421
50 nm (JMW1160)	49.1	54.3	418	43.86 [3.74]	43.00	0.89	420
60 nm (DAC1183)	57.4	66.7	429	56.97 [3.55]	56.13	0.78	431
70 nm (DAG1293)	68.5	69.0	441	64.11 [7.58]	63.30	0.87	443
80 nm (EAW1153)	77.9	82.7	457	74.76 [7.65]	73.41	0.86	459
80 nm (JMW1070)	78.9	75.9	457	75.06 [4.35]	74.33	0.91	458
100 nm (JMW1147)	99.4	97.7	491	95.33 [6.91]	94.42	0.87	491

[a/b]estimated from a log-normal fit of HR-TEM particle size count by [a]volume-weighted or [b]number-weighted distribution.

[c] the circularity equal 4π*area/perimeter^2. A value of 1.0 indicates a perfect circle.

[d] manufacturer's TEM size data was used for this sample

Manuf. = Manufacturer, NanoComposix Inc.

Definition S1. Definitions and calculations for concentration or extinction coefficient.

A absorbance

d_0 path length of light through the sample (usually 1cm for a cuvette)

c molar concentration of nanoparticles

ε molar decadic extinction efficiency (extinction coefficient)

m_{NP} mass of a single nanoparticle

N number density of nanoparticles

N_A Avogadro constant

A_r relative atomic mass (gold = 196.97, silver = 107.87)

V_{NP} volume of a nanoparticle

ρ density of nanoparticle material (gold = 1.93×10^4 kg/m^3, silver = 1.05×10^4 kg/m^3)

ω_p plasma frequency (138.0×10^{14} Hz)

ω_0 collision frequency (gold=0.333×10^{14} Hz, silver=0.274×10^{14} Hz)

υ_F Fermi velocity (1.38×10^8 cm/s)

τ_c static collision time (gold = 3.0×10^{-14} s, silver=3.65×10^{-14} s)

1) Beer-Lambert law: $A = c.\varepsilon.d_0$

2) Nanoparticle molar concentration: $c = N/N_A$

3) Number density of nanoparticles: $N = \frac{A}{\varepsilon} . N_A$

4) Mass of a single nanoparticle: $m_{NP} = V_{NP}.\rho$

5) The number of silver atoms per nanoparticle: $n_{Ag} = \frac{m_{NP}}{A_r}.N_A$

6) Molar mass of silver per sample: $$m_{Ag} = \frac{c.n_{Ag}}{A_r}$$

Figure S1. Exemplar electrode potentials for sodium cyanide concentrations between 0.1 mM and 1 mM, and its associated fit to the Nernst equation (black line) $E = E_o + S * \log (A)$, where E = measured electrode potential, E_o = reference potential, A = cyanide ion activity level in solution, and S = electrode slope.

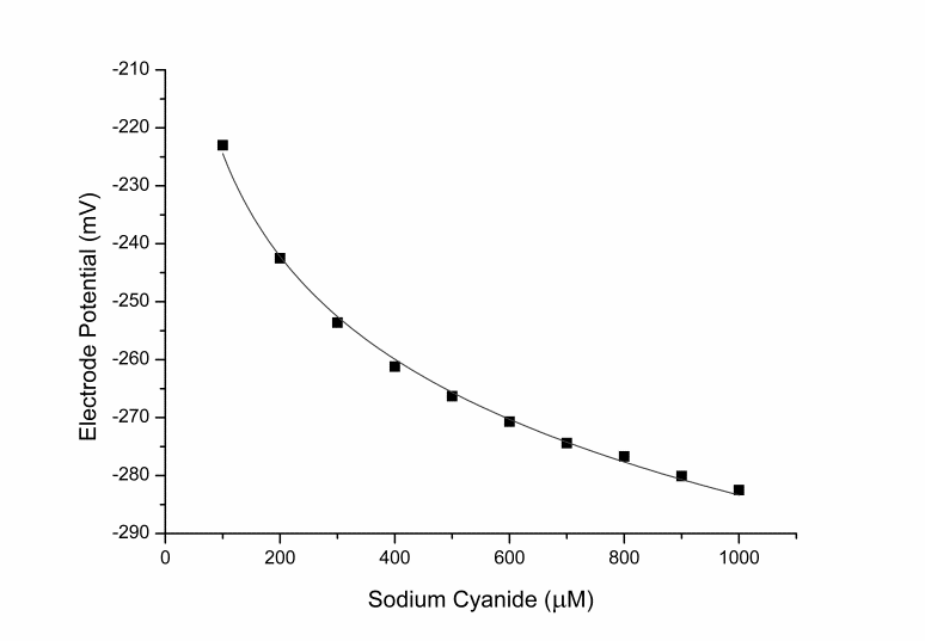

Figure S2. Molar ratio of consumed cyanide to gold for dissolved gold nanoparticles with mean sizes between 5.7 nm and 52.7 nm. A mean of 1.94 ± 0.16 was obtained from 25 experiments, data used in figure 1 is excluded.

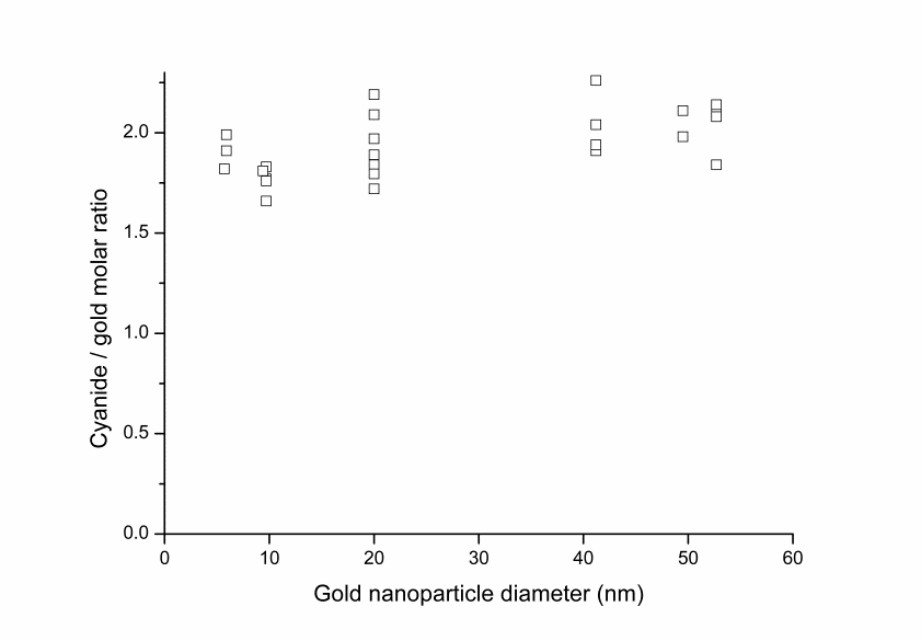

Figure S3. Comparison of size distribution by number-weighted and percentage volume-weighted distribution of 471 silver nanoparticles. The mean diameter by % volume distribution is 19.0 ± 1.8.

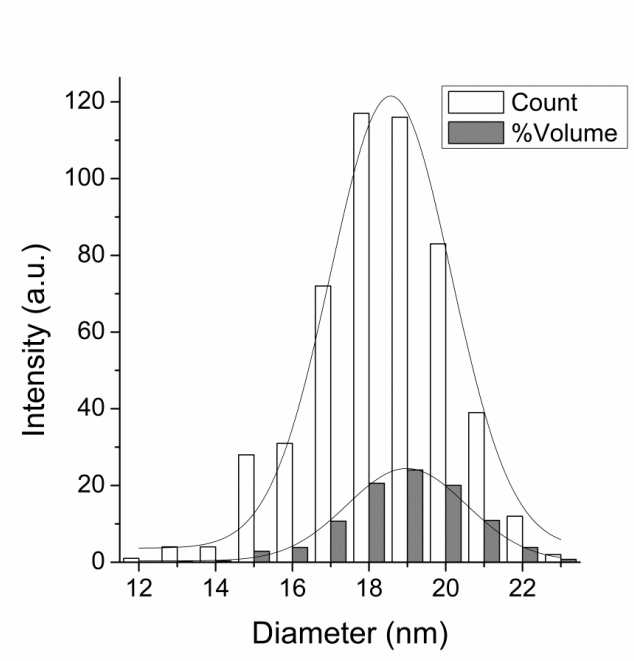

Figure S4. Exemplar UV-visible spectra of citrate-capped silver nanoparticles. Diameters of nanoparticles (expressed as %volume distribution, determined by HR-TEM) in increasing wavelength of λ_{max} are: 19.0 nm, 30.4 nm, 57.0 nm, 64.1 nm, and 95.3 nm, respectively.

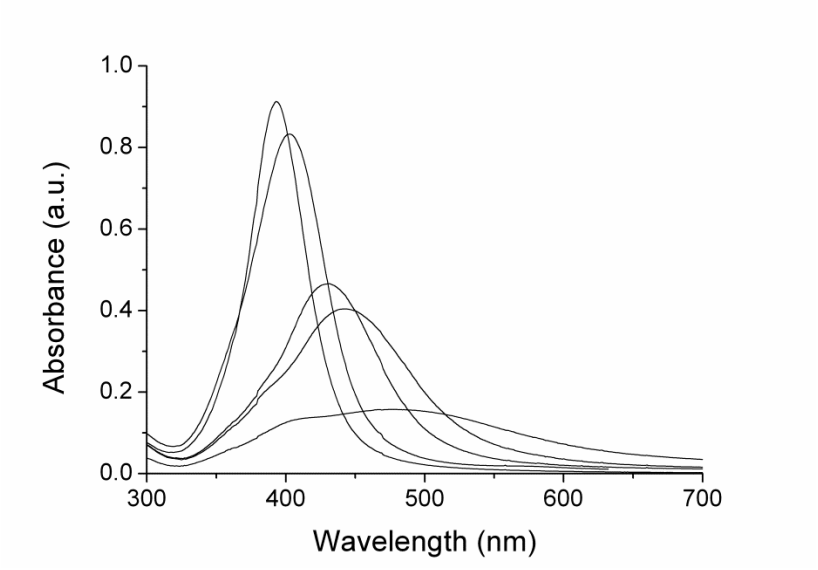
Absorbance (a.u.)
1.0
0.8
0.6
0.4
0.2
0.0
300
400
500
600
700
Wavelength (nm)

Figure S5a. Size distribution of 947 silver nanoparticles with average diameter of 8.9 ± 1.8 nm. The inset shows a typical TEM image used for calculations.

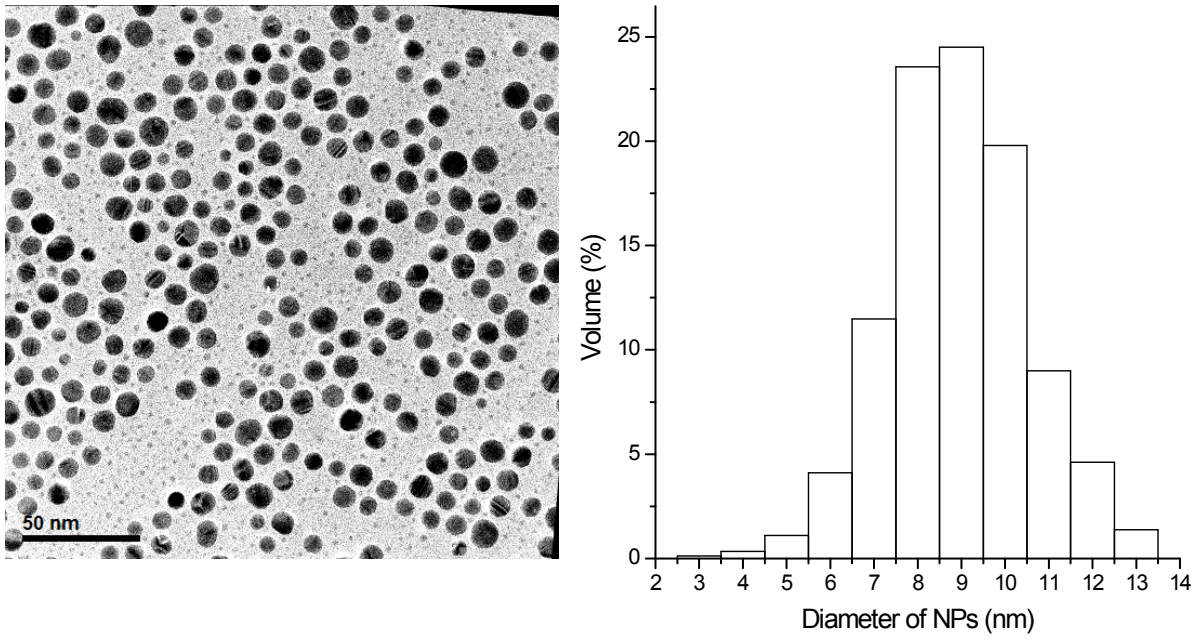

Figure S5b. Size distribution of 471 silver nanoparticles with average diameter of 19.0 ± 1.8 nm. The inset shows a typical TEM image used for calculations.

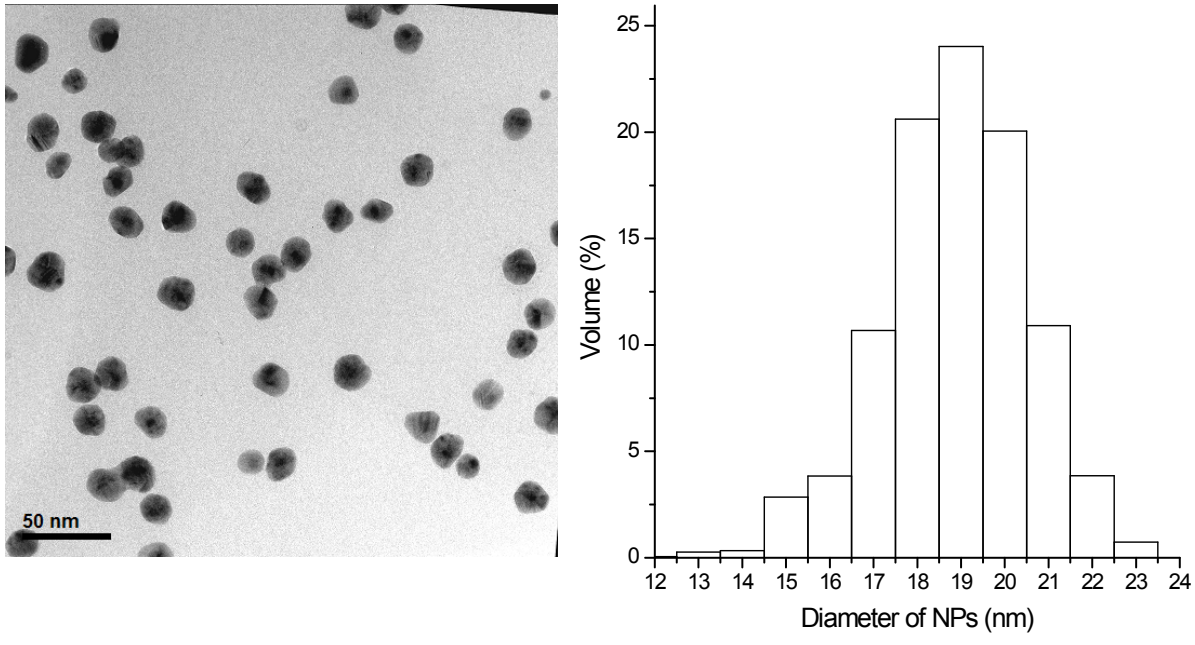

Figure S5c. Size distribution of 428 silver nanoparticles with average diameter of 19.8 ± 2.7 nm. The inset shows a typical TEM image used for calculations. Obtained images were not digitally modified, such as, for example, to remove the carbon grids shown in images S5c – S5l.

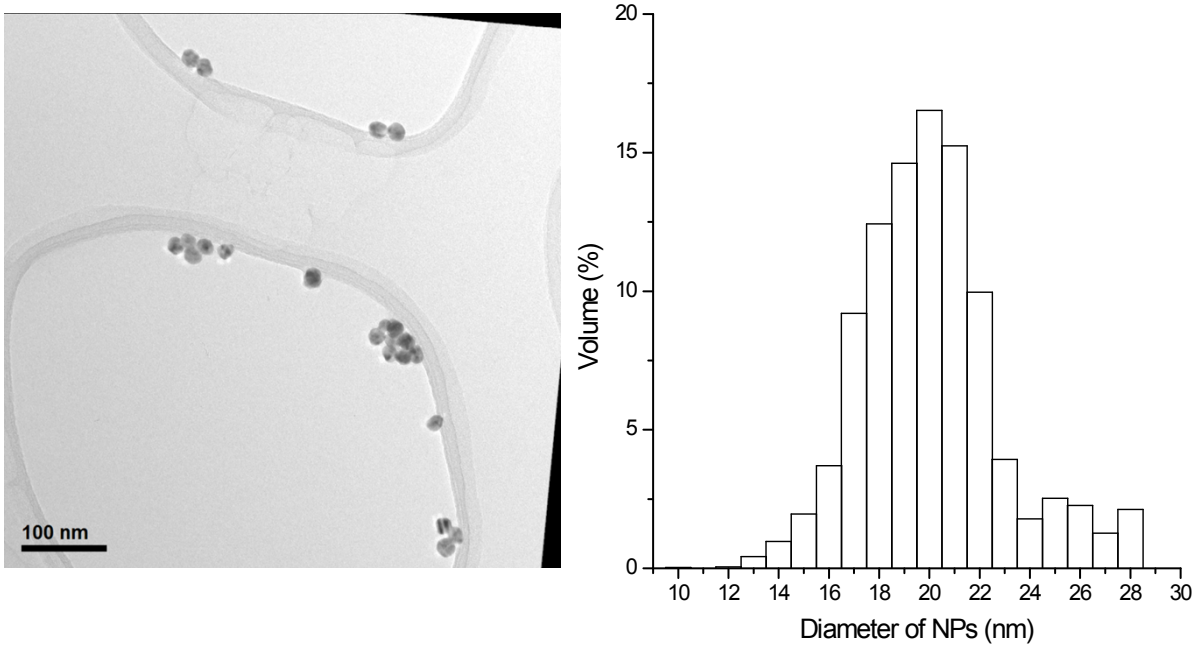

Figure S5d. Size distribution of 659 silver nanoparticles with average diameter of 30.4 ± 3.8 nm. The inset shows a typical TEM image used for calculations.

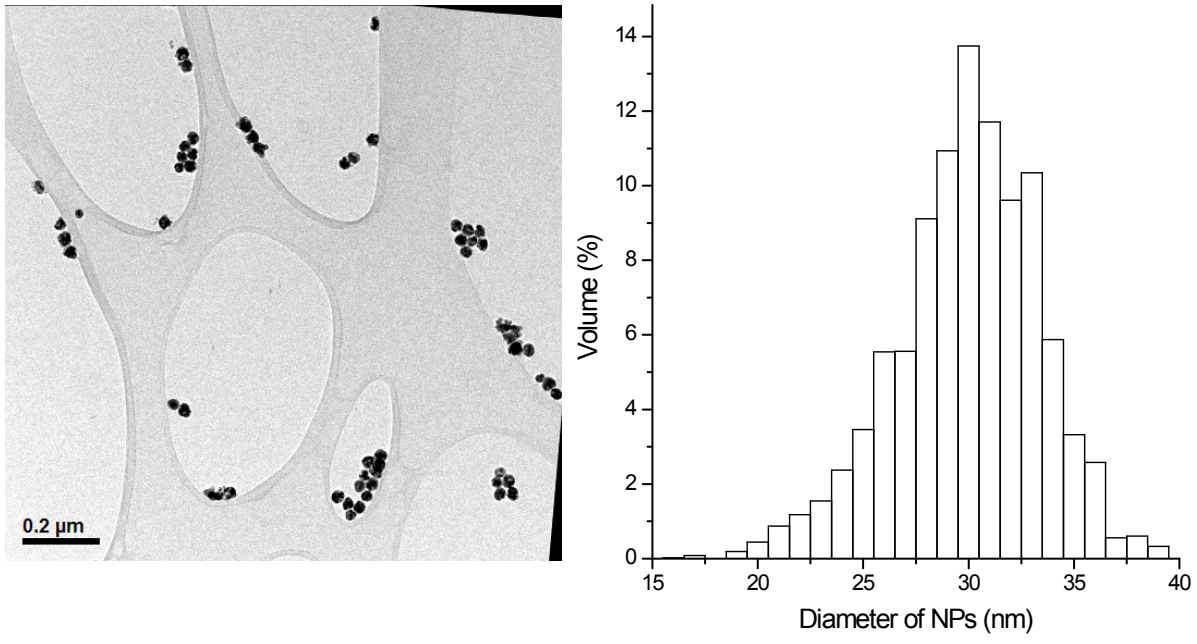

Figure S5e. Size distribution of 529 silver nanoparticles with average diameter of 37.9 ± 3.1 nm. The inset shows a typical TEM image used for calculations.

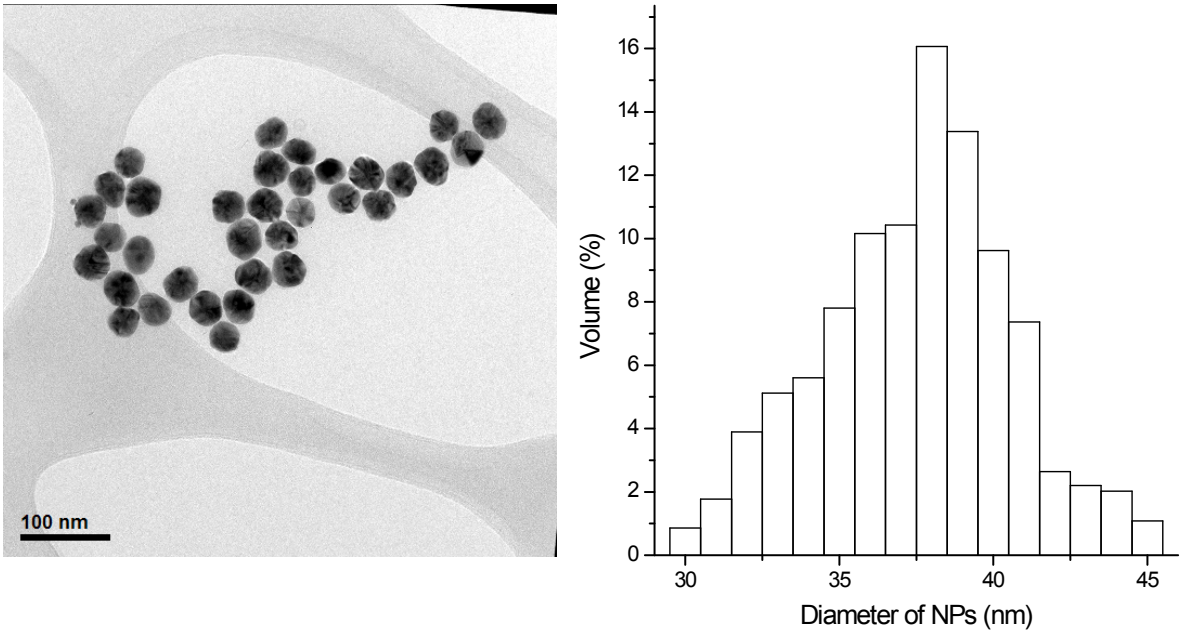

Figure S5f. Size distribution of 417 silver nanoparticles with average diameter of 45.9 ± 3.7 nm. The inset shows a typical TEM image used for calculations.

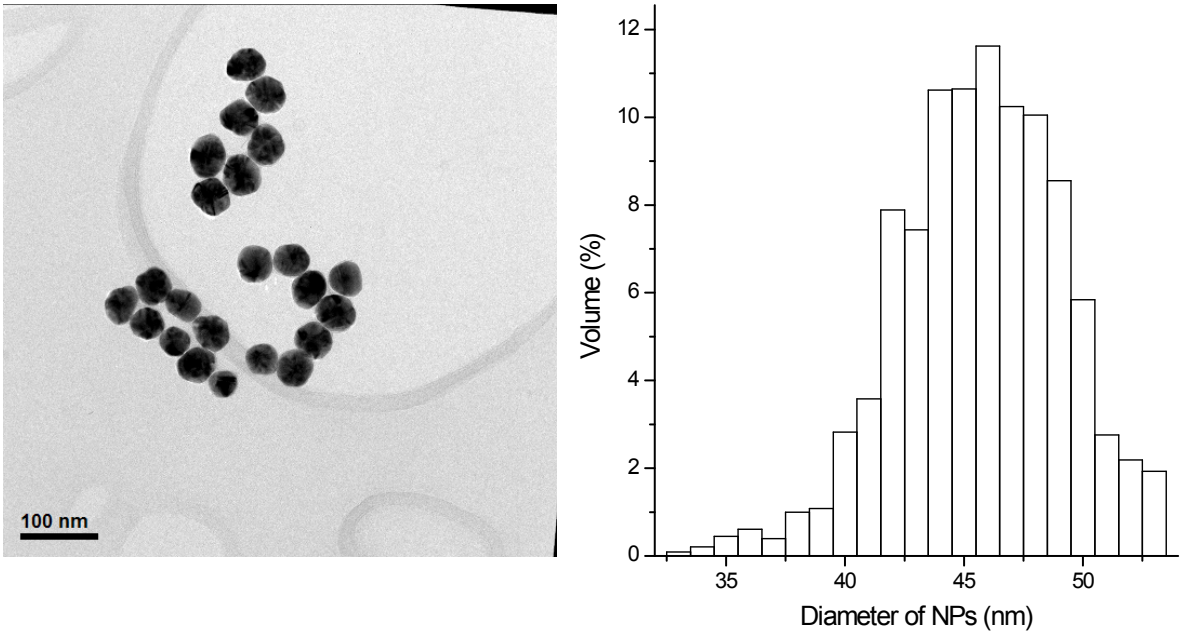

Figure S5g. Size distribution of 490 silver nanoparticles with average diameter of 43.9 ± 3.8 nm. The inset shows a typical TEM image used for calculations.

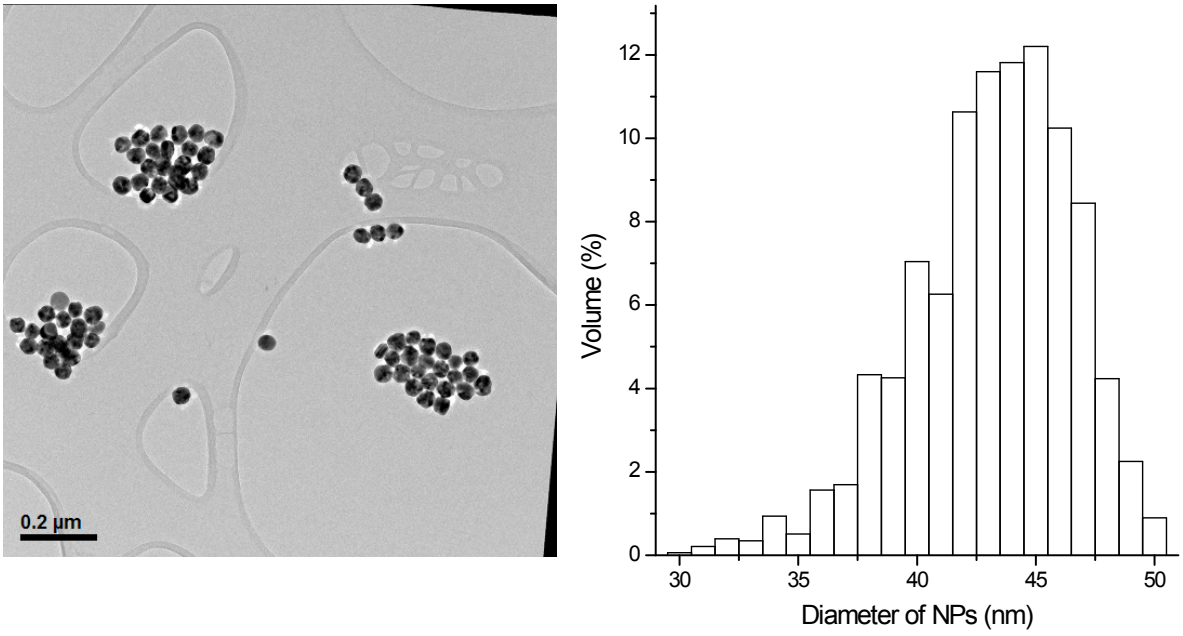

Figure S5h. Size distribution of 179 silver nanoparticles with average diameter of 56.9 ± 3.6 nm. The inset shows a typical TEM image used for calculations.

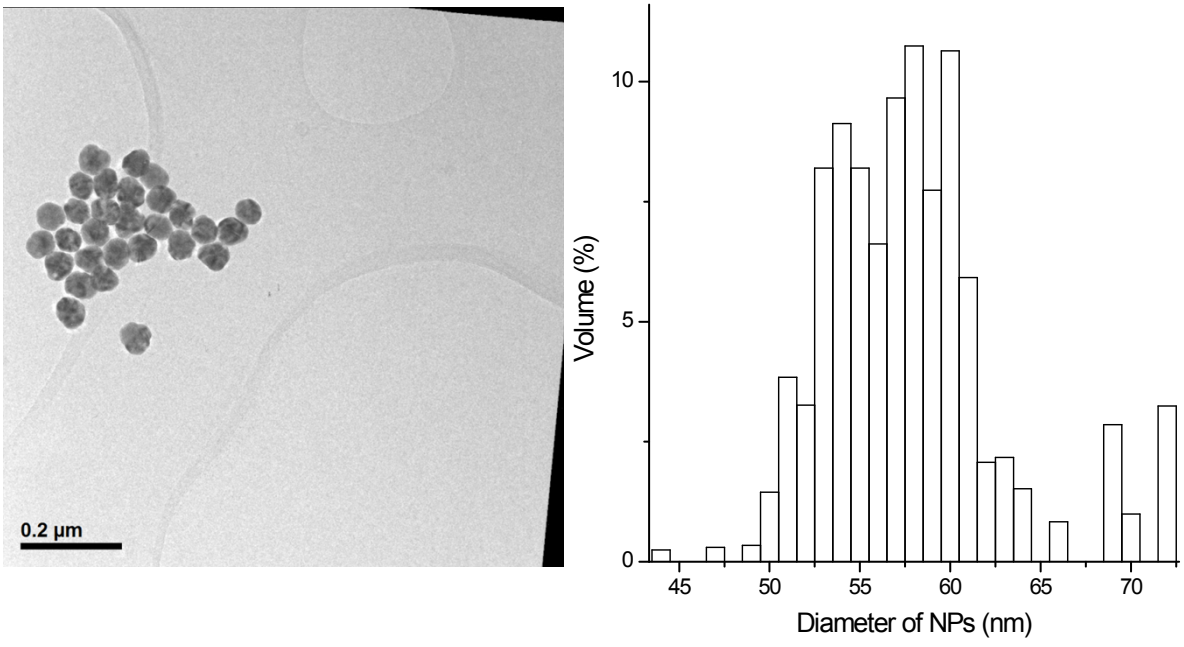

Figure S5i. Size distribution of 618 silver nanoparticles with average diameter of 64.1 ± 7.6 nm. The inset shows a typical TEM image used for calculations.

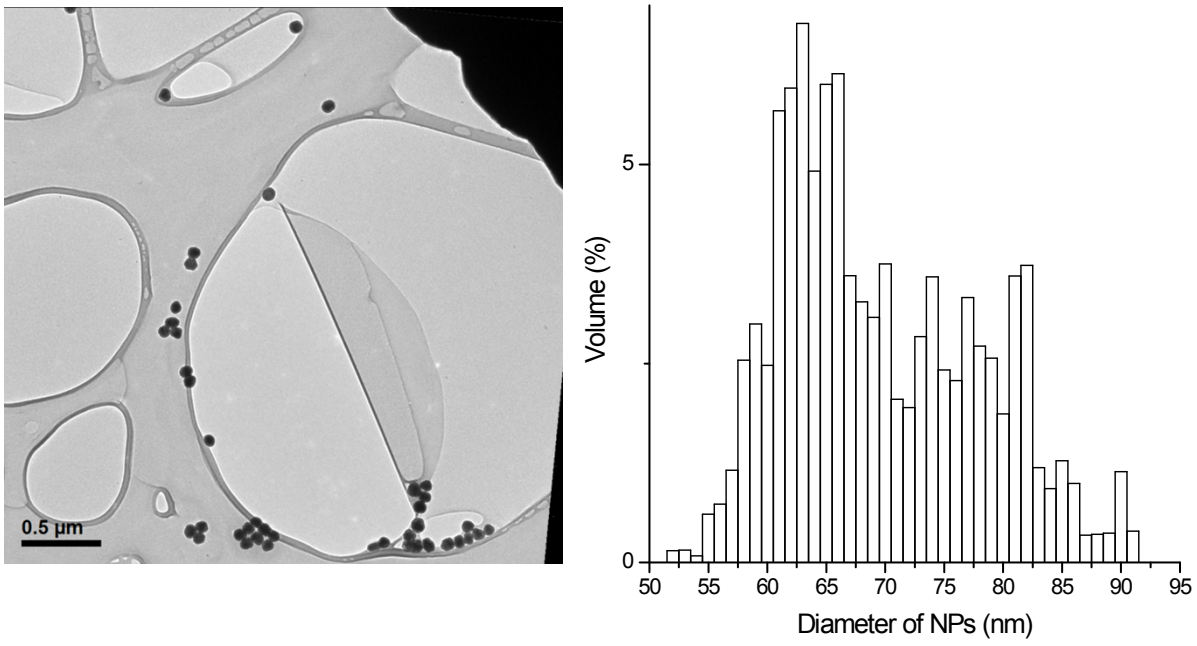

Figure S5j. Size distribution of 376 silver nanoparticles with average diameter of 74.8 ± 7.7 nm. The inset shows a typical TEM image used for calculations.

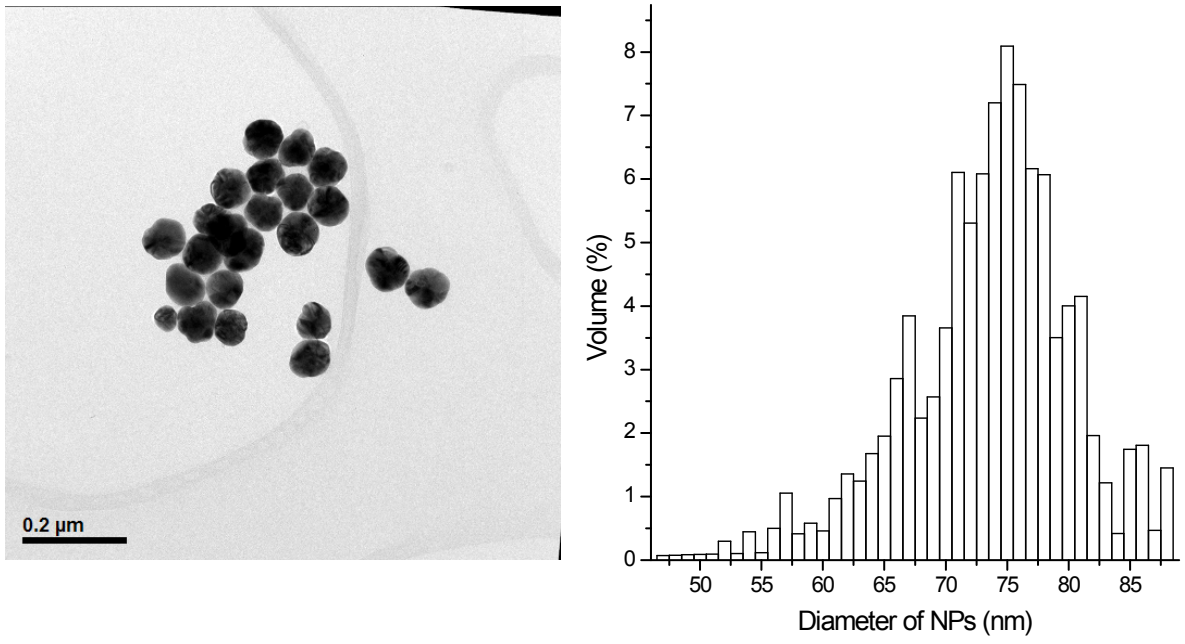

Figure S5k. Size distribution of 803 silver nanoparticles with average diameter of 75.1 ± 4.4 nm. The inset shows a typical TEM image used for calculations.

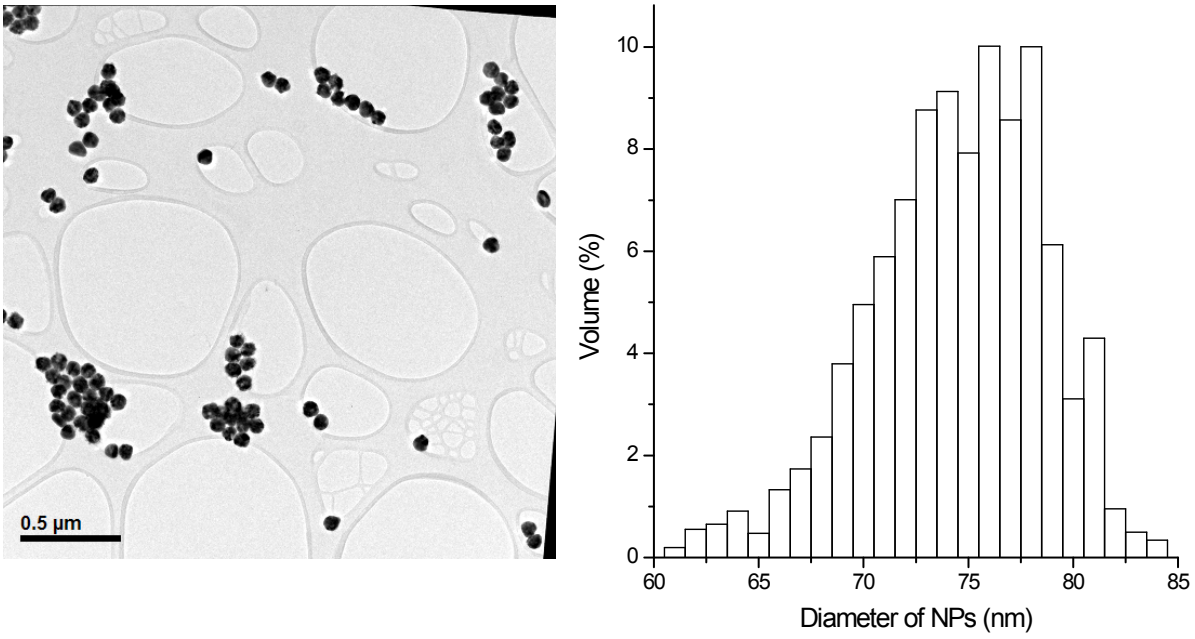

Figure S5l. Size distribution of 346 silver nanoparticles with average diameter of 95.3 ± 6.9 nm. The inset shows a typical TEM image used for calculations.

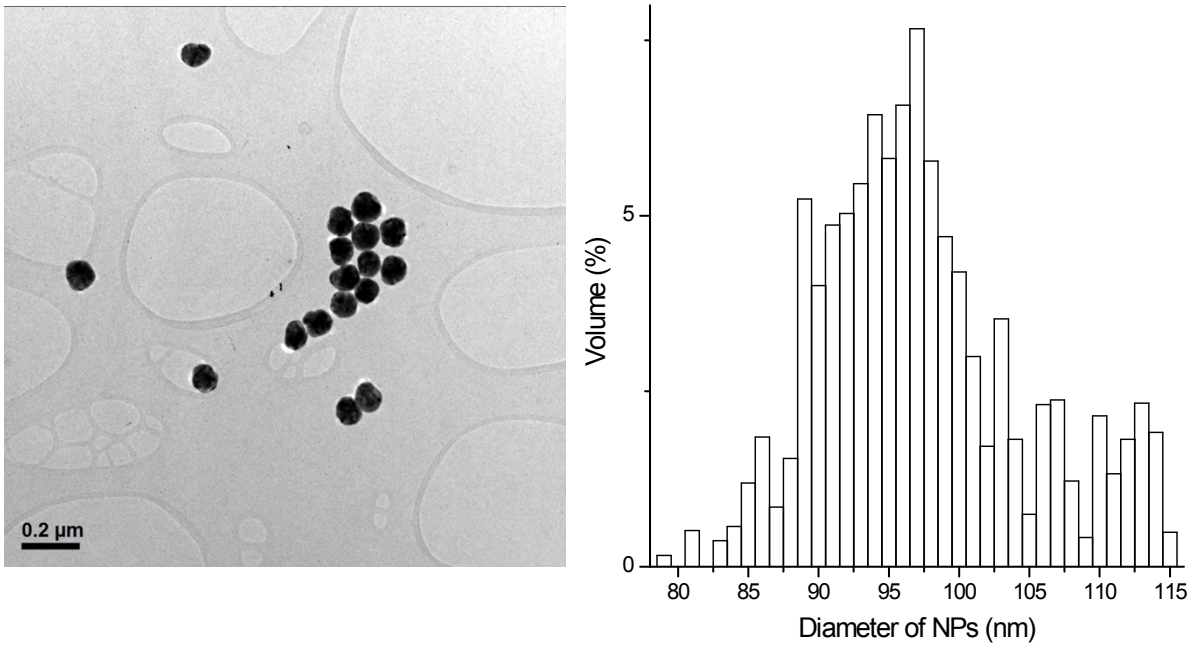

Figure S6. Comparison between intensity of maximum absorbance of solutions at different concentrations for measured (black squares) and simulated (black circles) absorbance for 45.9 nm nanoparticles.

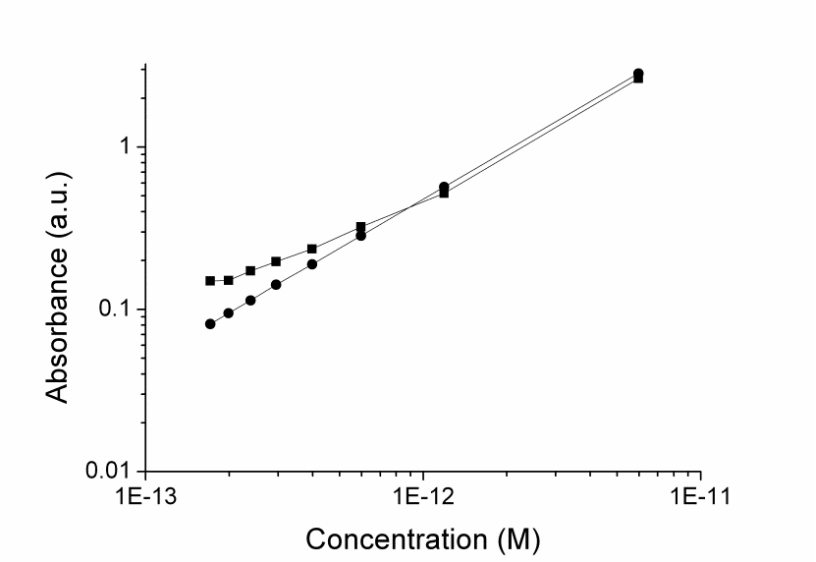

Figure S7. Intensity of maximum absorbance below 0.4 for 70 nm and 100 nm nanoparticles. Stock nanoparticles were concentrated and various dilutions of each sample plotted against absorbance. A linear fit was applied to samples with absorbance below 0.3 (open shapes). Absorbance above 0.3 (solid shapes) do not fit the linear correlation, probably due to an increased contribution of multiple scattering.

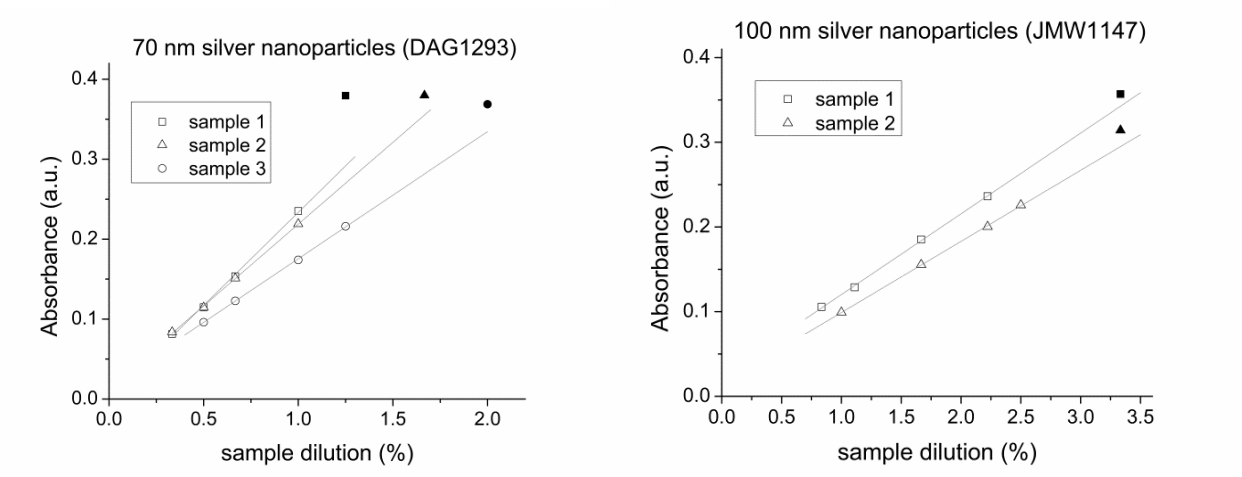

Figure S8. Analogous data to figure S7 but with y-axis expressed as integrated area below the UV-visible spectra between 340 nm and 650 nm.[1] A linear fit was applied to samples with an integrated area below 30 (open shapes). An integrated area value above 40 (solid shapes) does not fit the linear correlation.

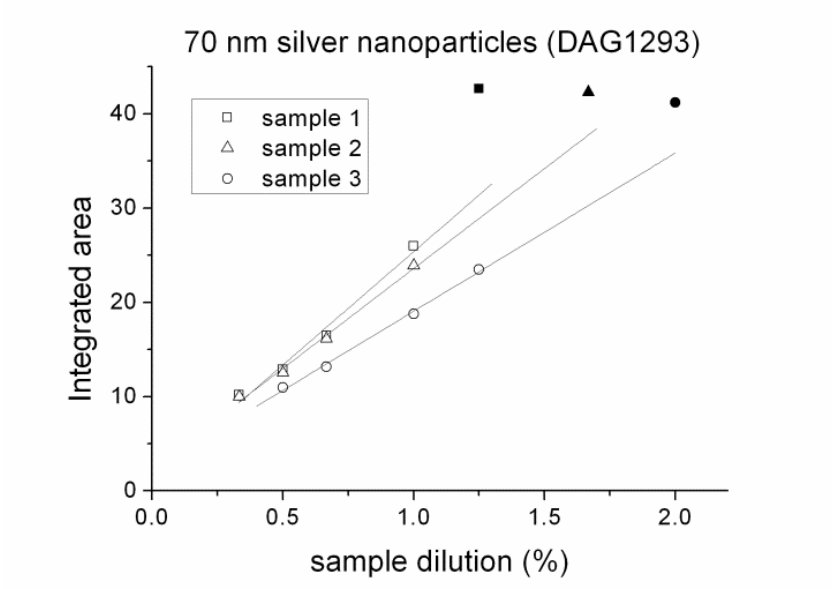

In figure 1 of Zook *et al*[1]. it was shown that the integration of the area beneath a UV-visible spectra is more accurate to determine relative dissolution of citrate-capped silver nanoparticles (at ~23 nm) than by comparing λmax values alone. We are not able to study this from our data or method, however we show for larger nanoparticles (S8) it is still essential to dilute below 0.3 absorbance even if expressing data as integrated area. Additionally this is not applicable to samples with changing UV-vis spectra due to capping for example. The samples shown in figure 6, had calculated integrated areas to be: Citrate only = 53.46, H-CALNN-OH = 26.36, PEG4 = 40.57, mix matrix = 42.38.

Definition S2. Simulation of silver nanoparticle extinction and definition of the contribution of dielectric constant and refractive index to the extinction efficiency of silver nanoparticles.

During the last two decades, calculations based on Mie's theory have been shown to be successful in simulations of optical spectra of nano and micro particles and have been further improved, for example by including multilayer capping for particles conjugated with biomacromolecules.[2] Also, effects of interfaces and substrates,[3–5] shape[6] and size,[7,8] on the extinction efficiency have been investigated. Mie's theory has also been implemented in different computer languages.[7,9–11] One of the essential parameters of Mie's theory is a dielectric constant of the material of a particle. Data for dielectric constants of silver nanoparticles has not to our knowledge been published. On the other hand, two sets of data on bulk silver optical constants are available[12,13] which can be used as the dielectric constant in the current study. This is because, for particles much larger in size than the electron mean free path in the bulk material the dielectric constant of the bulk material can be used. However, for particles less or similar to the electron mean free path in the bulk the dielectric constant should be modified taking into account the reduction of electron mean free path in the particle.[14].

Therefore, we calculated the bulk silver dielectric constant using optical constants reported by Johnson and Christy[12] and Palik,[13] and further modified them taking into account the electron mean free path reduction described above. The dielectric constants obtained from the two sets of data are shown in Figure S9. They are not equivalent, probably due to the difference in experimental methods used: both were measured on vacuum-evaporated thin films at room temperature, Johnson & Christy measured reflection and transmission at normal incidence and transmission of p-polarized light at 60° while Palik used reflectance measurements of synchrotron radiation and polarimetric measurements. To choose a suitable set of data in our case, we did a comparison between measured and simulated spectra of extinction efficiencies of silver nanoparticles of different sizes.

Figure S10 represents a comparison for silver particles of average diameter of 37.9 nm. Compared to experiment, Johnson and Christy's dielectric constant gives a blue shift of the spectrum of 11 nm, the intensity of the maximum peak is almost 2 times higher and furthermore, full width at half maximum (FWHM) = 21, compare to measured FWHM = 63 (Table S3). In contrast, the data published by Palik fits the experimental data with good agreement. Comparison of experimental and simulation data for 37.9 nm silver nanoparticles is shown in figure S10. Therefore, the dielectric constant of silver published by Palik has been used here. The extinction efficiency for other sizes of silver nanoparticles simulated with Palik's dielectric constant are shown in Figure S11.

The extinction efficiency Q_{ext} is determined as $Q_{ext} = \sigma_{ext}/\pi R^2$, where σ_{ext} is the extinction cross section and R is the nanoparticles radius.[7,9] The molar decadic extinction coefficient is related to the extinction cross section as $\varepsilon = \sigma_{ext} \cdot N_A/(1000\ln(10))$ and the experimentally measured "Absorbance" (-log (Transmittance)) is $A = c\varepsilon d_0$ where d_0 is the path length of light through the sample, which is equal to 1 cm, c is the molar concentration of the nanoparticles, and N_A is Avogadro's constant. Experimental and simulated maximum extinction efficiency wavelengths for different nanoparticle diameters are shown in figure S12. Again we did simulation of the extinction efficiency using the dielectric constant published by Palik and Johnson & Christy. As we

mentioned above, simulation based on Johnson and Christy's constant gives a blue shift around 11 nm, whereas simulation based on Palik's constant gives a very good fit of the experimental data obtained with nanoparticles of diameter 20.0 nm to 75.0 nm.

To introduce reduction of the mean free path of conduction electrons, the complex dielectric constant $\varepsilon = \varepsilon^{''} + i\varepsilon''$ should be split into contribution of the bound (B_1 and B_2) and free ($A_1(R)$ and $A_2(R)$) electrons

$$\varepsilon(R) = \left(A_1(R) + B_1\right) + i\left(A_2(R) + B_2\right),$$

$$A_1(R) = 1 - \frac{\omega_p^2}{\omega^2 + \omega_0(R)^2},$$

$$\mathrm{A}_2(R) = \frac{\omega_p^2 \omega_0(R)^2}{\omega\left(\omega^2 + \omega_0(R)^2\right)},$$

where $\omega_p = \left(4\pi N_c e^2/m^*\right)$ is the plasma frequency with the density of conduction electrons N_c, the electron charge e, and the effective mass of conducting electron m^*.

The collision frequency ω_0 considering reduction of the mean free path could be found from

$$\omega_0(R) = 1/\tau_s + \upsilon_F/R,$$

where τ_s is the static collision time in bulk and υ_F is the Fermi velocity. Ratio R/υ_F represents the contribution to the collision time in the case when the electrons collide with the surface of the small nanoparticle.[12,15,16] Parameters B_1 and B_2 represent contribution of bound electrons which are independent of particle size. They could be extracted from the complex dielectric constant of bulk silver

$$\hat{\varepsilon} = \left(A_1 + B_1\right) + i\left(A_2 + B_2\right)$$

where A_1 and A_2 are solved as above, using the collision frequency and the dielectric constant of bulk silver, $\omega_0 = \frac{1}{\tau_s}$ and $\hat{\varepsilon} = \varepsilon^{'} + i\varepsilon^{''}$, accordingly.

Thus dielectric constant dependence of wavelength for silver nanoparticles is highly important data for the simulation. The real ε' and imaginary ε'' components of the dielectric constant $\hat{\varepsilon}$ could be found from the next equations:

$$\varepsilon' = n^2 + k^2$$

$$\varepsilon^{''} = 2nk$$

where n is the refractive index of silver, and k is the wave vector $k = 2\pi/\lambda$. In other words the complex refractive index $\hat{n} = n + ik$ and the complex dielectric constant $\hat{\varepsilon} = \hat{n}^2$. Parameters n and k values of materials depend on the wavelength.

Figure S9. Real ε' and imaginary ε'' components of the dielectric function $\hat{\varepsilon}$ of bulk silver published by Johnson & Christy[12] and Palik.[13]

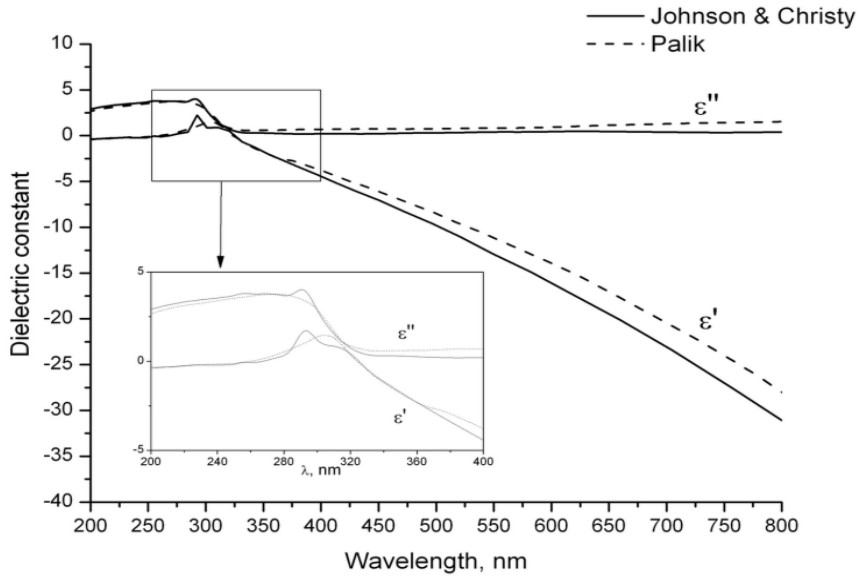

Table S3. Comparison between experimental and simulated data of 37.9 nm silver nanoparticles of concentration 43 pM.

	λ_{max}, nm	Q_{ext} at λ_{max}	FWHM, nm
Experimental data	411.0	8.8	63
Simulation with Palik's ε	411.2	9.6	51
Simulation with J&Ch's ε	397.2	17.2	21

Figure S10. Extinction efficiency of 37.9 nm silver nanoparticles at 43 pM, of experimental data (solid line), simulated absorbance using dielectric constant published by Johnson & Christy[12] (dashed line) and simulated absorbance using dielectric constant published by Palik.[13] (dotted line).

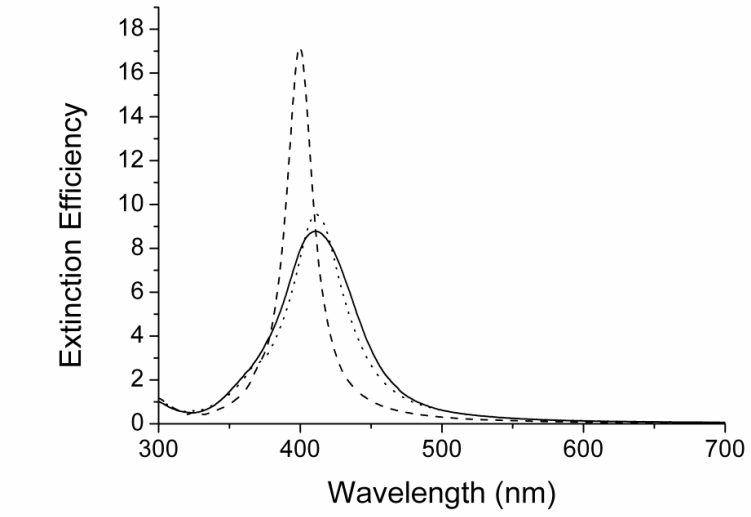

Figure S11. Extinction efficiency of silver nanoparticles simulated using the dielectric constant published by Palik.[13]

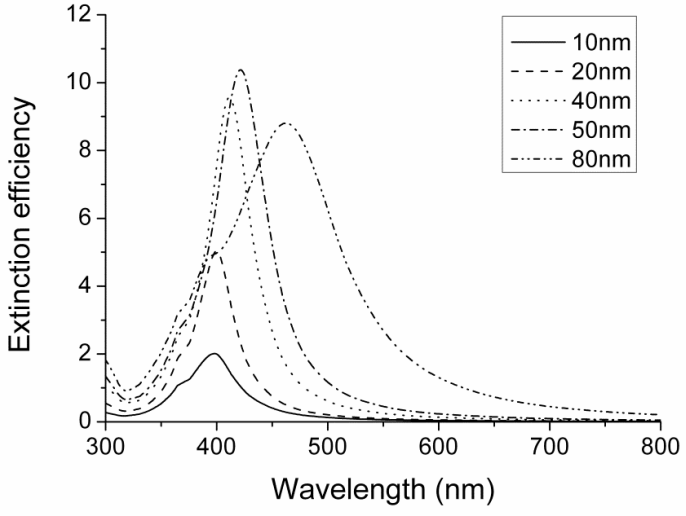

Figure S12. Wavelength of maximum absorbance of different silver nanoparticles sizes for experimental (black square) and simulated data using Palik's[13] (empty circle) or Johnson and Christy's[12] (empty triangle) data.

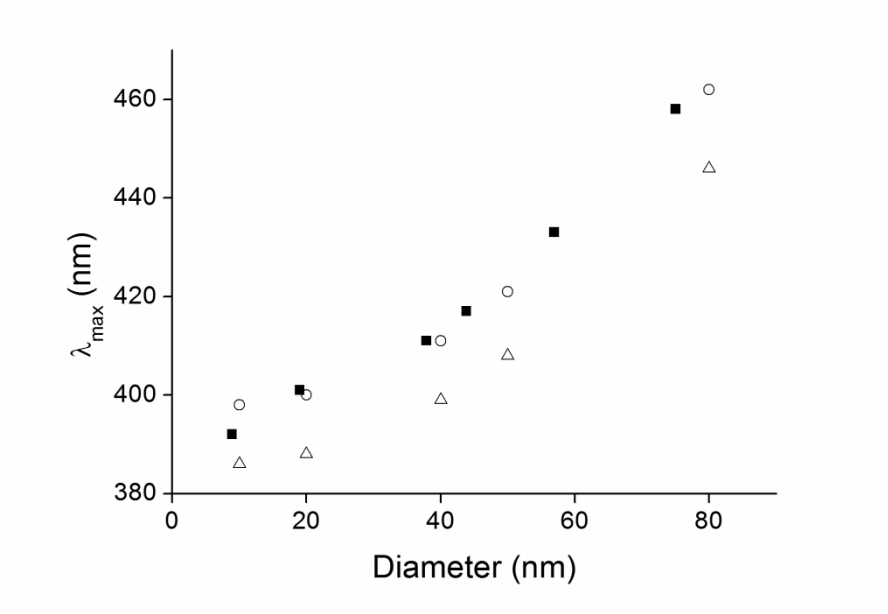

Figure S13. Comparison of simulated (75.0 nm) and experimental (75.1 nm) spectra from silver nanoparticles. Data is normalized for absorbance at the λ_{max} wavelength value.

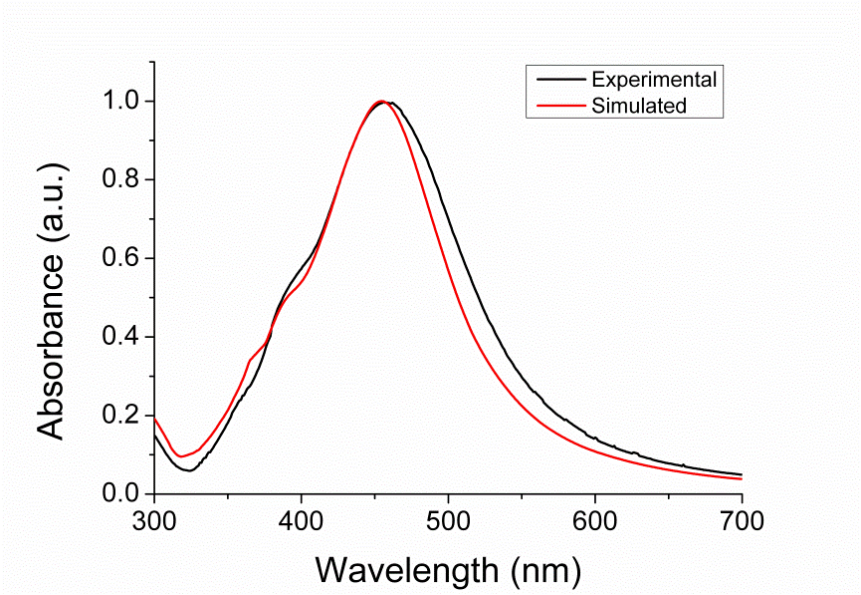

Figure S14. Molar decadic extinction coefficient calculated based upon nanoparticle size expressed from HR-TEM number-weighted distribution or % volume-weighted distribution.

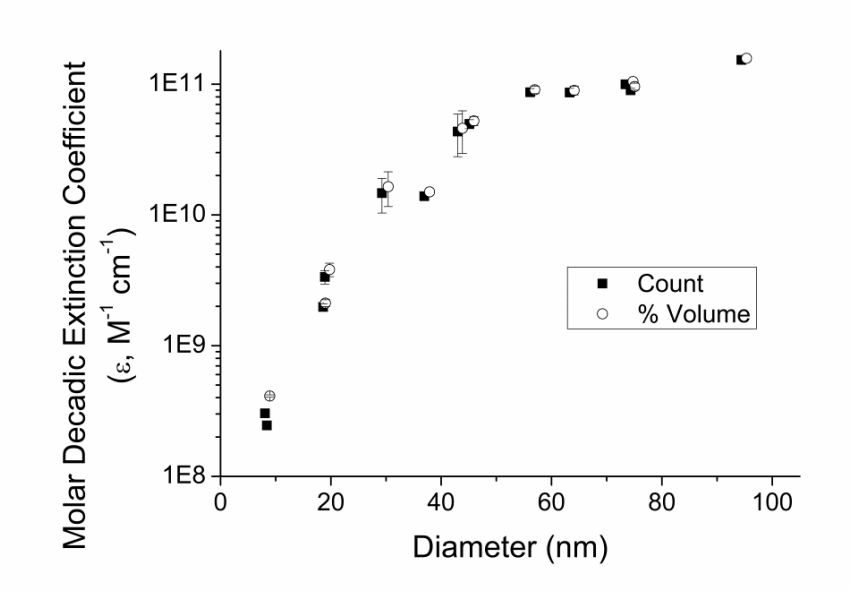

Figure S15. Example comparative spectra of citrate-capped 44 nm silver nanoparticles using a Molecular Probes Spectramax 384, Shimadzu UV-3600, and an Ocean Optics USB-4000.

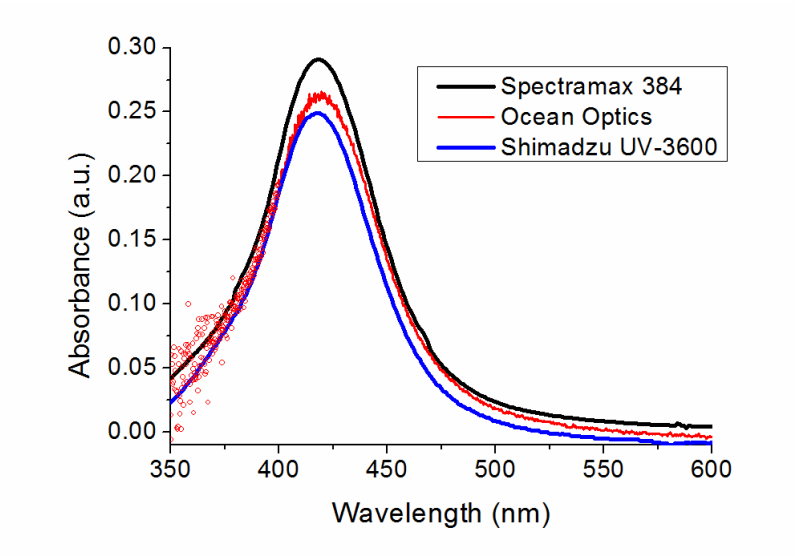

The measurement of absorbance is internally consistent for a range of spectrometers with different light sources and detector sensitivity. This is because the absorbance is the logarithm of the ratio of the incident light to the transmitted light. However the sensitivity of the spectrometer at any given wavelength will be governed by the lamp stability and the combined effect of the lamp power and detector response. The spectrometer should have sufficient response and lamp intensity in the wavelength range where the measurement is being made so that the noise does not mask the signal. A good example of this is shown above in figure S15. For the Ocean Optics spectrometer the lamp intensity below 400nm is a bit low and this leads to increased noise in the spectrum in that region. Lamp stability will limit the lowest concentrations that can be measured as the number of photons being absorbed can become similar to the lamp fluctuation at sufficiently low absorbances.

Values of absorbance are dependent on spectroscopic measurement parameters, including the spectrometer slit width (in our case the slit width was 2nm) and an appropriate baseline being set. The wider the slit width the more broadening of the peak may occur, however we found that varying the slit width (0.5nm, 2nm and 8nm) on a Shimadzu UV-3600 had minimal changes to the spectra. We tested five separate samples (4 x 50 nm, 1 x 80 nm) for absorbance on three different spectrometers (Spectramax 384, Shimadzu UV-3600, and Ocean Optics USB-4000) and found a difference in maximum absorbance with S.D. of 5.8% between these instruments, and all samples settled satisfactorily close to baseline. We would recommend that baseline normalisation at 1000nm be performed should baseline not be reached. It is thus important to use the same spectrometer and quartz cuvette (with same alignment) for all measurements.

References

1. J. M. Zook, S. E. Long, D. Cleveland, C. L. A. Geronimo, and R. I. MacCuspie, *Anal. Bioanal. Chem.*, 2011, **401**, 1993–2002.
2. N. G. Khlebtsov, *J. Quant. Spectrosc. Radiat. Transf.*, 2004, **89**, 143–153.
3. A. Curry, G. Nusz, A. Chilkoti, and A. Wax, *Opt. Express*, 2005, **13**, 2668–2677.
4. A. Hilger, N. Cűppers, M. Tenfelde, and U. Kreibig, *Eur. Phys. J. D.*, 2000, 115–118.
5. N. Nitin, D. J. Javier, D. M. Roblyer, and R. Richards-kortum, *J. Biomed. Opt.*, 2007, **12**, 051505:1–10.
6. A. Centeno, J. Breeze, B. Ahmed, H. Reehal, and N. Alford, *Opt. Lett.*, 2010, **35**, 76–78.
7. C. F. Bohren and D. R. Huffman, *Absorption and Scattering of Light by Small Particles*, Wiley-VCH Verlag GmbH, Weinheim, Germany, 1998.
8. D. C. Skillman and C. R. Berry, *J. Opt. Soc. Am.*, 1973, **63**, 707–713.
9. W. Haiss, N. T. K. Thanh, J. Aveyard, and D. G. Fernig, *Anal. Chem.*, 2007, **79**, 4215–4221.
10. S. Prahl, Oregon Medical Laser Center, Mie Scattering Calculator, http://omlc.ogi.edu/calc/mie_calc.html, (accessed May 2014).
11. P. Zakharov, phpMie: Online Mie Scattering Calculator for Spheres, http://zakharov.zzl.org/lstar.php, (accessed May 2014).
12. P. B. Johnson and R. W. Christy, *Phys. Rev. B*, 1972, **6**, 4370–4379.
13. E. D. Palik, Ed., *Handbook of Optical Constants of Solids*, Academic Press, New York, 1985.
14. U. Kreibig and C. Z. Vonfrags, *Z. Phys.*, 1969, **224**, 307–323.
15. R. G. Driggers, *Encyclopedia of Optical Engineering*, Marcel Dekker, New York, Volume 3., 2003.
16. H. Ehrenreich and H. Philipp, *Phys. Rev.*, 1962, **128**, 1622–1629.